has found wide acceptance[17,18]. But for its higher melting point (70.6°C), which necessitates quick dispensing[8], isubgol is a cost-effective gelling agent with desirable properties[9]. Gum Katira, like ficoll, does not form a firm gel at 3%, but the explants remain on the surface if left undisturbed. In transparency, Gum Katira-gelled medium is comparable to the liquid medium. Therefore, it can be an excellent gelling agent for experiments requiring regular observations of cells, tissues or organs growing inside the medium[9].

As cost of isubgol and guar gum per litre of the medium is about 2.5–13 times less than different brands of agar (Table 2), these are two highly cost-effective gelling agents, which could be used for reducing the cost of *in vitro*-propagated orchids plants. Both being of plant origin, are biodegradable and do not pose any threat to the environment on being dispensed-off after use. Moreover, both *P. ovata* and *Cyamopsis tetragonoloba*, sources of isubgol and guar gum respectively, are easily cultivated and therefore, their increased demands can be easily met. However, media gelled with isubgol or guar gum, require quick adjustment of pH and dispensing because of their higher gelling point.

1. Ahuja, P. S. *et al*., Commercialization of Indian orchids. In *Orchids: Science and Commerce* (eds Pathak, P. *et al.*), Bishen Singh Mahendra Pal Singh Publ., Dehradun, 2001, pp. 451–458.
2. Prakash, D. and Chaudhary, M. L., *In vitro* multiplication of orchids. In *Orchids: Science and Commerce* (eds Pathak, P. *et al.*), Bishen Singh Mahendra Pal Singh Publ., Dehradun, 2001, pp. 363–381.
3. Pelczar, Jr. M. J. *et al.*, *Microbiology*, McGraw Hill, Singapore, 1986.
4. Kohlenbach, H. W. and Wernicke, W., Investigations on the inhibitory effect of agar and the function of active carbon in anther culture. *Z. Pflanzenphysiol.*, 1978, **86**, 463–472.
5. Singha, S., Influence of two commercial agars on *in vitro* shoot proliferation of 'Almey' crabapple and 'Seckel' pear. *Hortic. Sci.*, 1984, **19**, 227–228.
6. Johansson, L. *et al.*, Improved anther culture technique: activated charcoal bound to the agar medium in combination with liquid medium and elevated CO_2 concentration. *Physiol. Plant.*, 1982, **54**, 24–30.
7. Jain, N. *et al.*, Isubgol as an alternative gelling agent for microbial culture media. *J. Plant Biochem. Biotechnol.*, 1997, **6**, 129–131.
8. Babbar, S. B. and Jain, N., 'Isubgol' as an alternative gelling agent for plant tissue culture media. *Plant Cell Rep.*, 1998, **17**, 318–322.
9. Jain, N. and Babbar, S. B., Gum Katira – a cheap gelling agent for plant tissue culture media. *Plant Cell Tissue Org. Cult.*, 2002, **71**, 223–229.
10. Mitra, G. C. *et al.*, Inorganic salts and differentiation of protocorms in seed-callus of an orchid and correlated changes in its free amino acids. *Indian J. Exp. Biol.*, 1976, **14**, 350–351.
11. Vij, S. P. *et al.*, Orchid micropropagation. In *Biotechnology in Horticultural and Plantation Crops* (eds Chadha, K. L., Ravindran, P. N. and Sahijram, L.), Malhotra Publ. House, New Delhi, 2000, pp. 598–641.
12. Tremblay, L. and Tremblay, F. M., Effects of gelling agents, ammonium nitrate and light on the development of *Picea mariana* (Mill.) B. S. P. (black spruce) and *Picea rubens* Sarg. (red spruce) somatic embryos. *Plant Sci.*, 1991, **77**, 233–242.
13. Johansson, L. B., Increased induction of embryogenesis and regeneration in anther cultures of *Solanum tuberosum* L. *Potato Res.*, 1988, **31**, 145–149.
14. Scheurich, P. *et al.*, Immobilization and mechanical support of individual protoplasts. *Biochim. Biophys. Acta*, 1980, **598**, 645–651.
15. Bromke, B. J. and Furiga, M., Carrageenan is a desirable substitute for agar in media for growing *Trichomonas vaginalis*. *J. Microbiol. Methods*, 1991, **13**, 61–65.
16. Kao, K. N., Plant formation from barley anther cultures with ficoll media. *Z. Pflanzenphysiol.*, 1981, **103**, 437–443.
17. Pasqualetto, P. L. *et al.*, The influence of cation and gelling agent concentration on vitrification of apple cultivars *in vitro*. *Plant Cell Tissue Org. Cult.*, 1998, **14**, 31–40.
18. Eyre, M. J. and Caswell, E. P., Sterile culture of *Rotylenchulus reniformis* on tomato root with gellan gum as a supporting medium. *J. Nematol.*, 1991, **23**, 229–231.

ACKNOWLEDGEMENT. We thank Prof. S. P. Vij, Department of Botany, Panjab University, Chandigarh for providing cultures of *Dendrobium chrysotoxum*.

Received 19 June 2004; revised accepted 14 September 2004

Spectral attenuation models in the Sikkim Himalaya from the observed and simulated strong motion events in the region

Sankar Kumar Nath*, Madhav Vyas, Indrajit Pal, Avinash Kumar Singh, Sudeshna Mukherjee and Probal Sengupta
Department of Geology and Geophysics, Indian Institute of Technology, Kharagpur 721 302, India

Strong motion recordings by the Sikkim Strong Motion Array (SSMA) of 80 events with good signal-to-background noise ratio (≥ 3) for magnitude between 3 to 5.6, have enabled estimation of source model and site response, and also the simulation of spectral acceleration for moderate-to-large earthquakes with $6 \leq M_W \leq 8.3$. A combined simulated and recorded data set have ultimately been utilized for deriving the spectral attenuation laws incorporating the local site conditions, namely, topographic effect and site response, with and without shear wave velocity in addition to the normal earthquake parameters, viz. moment magnitude (M_W) and source-to-site distance (r). The spectral attenuation laws developed in this study have been found to be appropriate for predicting free-field horizontal Peak Ground Acceleration (PGA) for earthquakes of $3 \leq M_W \leq 8.3$ and for the sites with distances up to 100 km from the source in the Sikkim Himalaya. The estimated spectral acceleration through these attenuation laws mimic the mean spectral acceleration simulated using Brune's source model.

THE Sikkim Himalaya located in the northeastern Indian Peninsula, is seismically one of the six most active regions

*For correspondence. (e-mail: nath@gg.iitkgp.ernet.in)

of the world, being placed at the boundary of seismic zone V (PGA > 0.4 g), the highest region of the seismic zonation map of India (IS1893-2002). The high seismicity in the region is attributed to the collision tectonics between the Indian plate and the Eurasian plate to the north and Indo-Myanmar range to the east. There can be different methods of quantifying risk and hazard in a region, one of those being the estimation of Peak Ground Acceleration (PGA) through empirically developed attenuation relationships for the prediction of design ground motions that is often controlled by a hypothesized occurrence of a large earthquake on a nearby fault. Among the studies that characterize the Himalayan region of the country, the works that demand mention are those of the attenuation relationship based on multiple regression approach of Sharma[1] and the one derived by Parvez *et al.*[2] through combination of observations with theoretically based attenuation laws. Both Sharma[1] and Parvez *et al.*[2] used the strong motion array installed in the Himalayan region. The present study describes a set of attenuation relationships that we specifically developed to predict horizontal component of PGA and the spectral acceleration (SA) in the near source region using strong motion recordings of 80 events with magnitude (M_L) between 3 to 5.6 and large events through spectral simulation assuming Brune's source model with magnitude between 6 and Maximum Credible Earthquake [MCE from Global Seismic Hazard Assessment Program (GSHAP) considerations][3] of magnitude 8.3. Initially a local relationship was established wherein we considered PGA to be a function of magnitude and distance only starting with a generalized attenuation law[4]. It has been considered prudent to ameliorate the relationship by incorporating corresponding terms for elevation, site response and shear wave velocity. Over the last two decades many researchers studied ground motion attenuation relationships that are, in essence, multiple regression models permitting predictions of a target parameter by means of an empirical relationship established on the basis of available strong motion data from a particular region. The engineering models that directly predict ground motion amplitude or that predict the modulation of this amplitude from such effects as fault geometry, source directivity and local site conditions in the form of a single coherent set of attenuation relationships are kept in mind while attempting the present analysis. The attenuation models of Joyner and Boore[5,6], Campbell[7] and Fukushima and Tanaka[8] have been considered for establishing the attenuation relationship for the horizontal component of PGA. The strong motion parameters considered here include the horizontal PGA, spectral acceleration (SA), earthquake magnitude (M_W), source-to-site distance (r), local site condition (S_V and S_R) and station elevation or topography (h). Moment magnitude (M_W), a better measure of the true size[9] of an earthquake is used to define earthquake magnitude in the present study. Source-to-site distance (r) is defined as the shortest distance between the recording site and the presumed zone of seismogenic rupture on the fault; the same is also referred to as hypocentral distance in case of a point source assumption.

To quantify the effects of local site conditions we have used two parameters namely Shear Wave Velocity (S_V) and Site Response (SR). The soil thickness at different sites was estimated through seismic refraction profiling using a 24-channel engineering seismograph. Site classification is done on the basis of shear wave velocity[10], which has been computed through the correlation of soil taxonomy map at 1 : 50,000 scale from National Bureau of Soil Survey[11] and couple of litho-logs. Being situated in a hilly terrain, the Sikkim region is found through seismic refraction survey to be devoid of a thick sediment cover and hence no term incorporating the thickness of the soil has been used in the present analysis. Instead, S_V and SR are used to represent and account for local site amplifications.

Topography plays a vital role for sites situated in a hilly terrain. In such areas, apart from incident wave we are expected to record diffracted and scattered waves that emanate from different parts of the hill which are hit upon by the incident waves. In regimes where constructive interference between incident and diffracted waves takes place, we observe site amplification and wherever destructive interference takes place amplitude gets reduced. This topographic effect, however, follows the frequency content of the signal as exhibited later in the site response analysis. A term for topography is, therefore, introduced in our attenuation models.

A semi-permanent 9-station strong motion array in Sikkim established by IIT, Kharagpur, India has been operative since 1998. One Kinemetrics Altus K2 and 8 Kinemetrics Altus ETNA high dynamic range strong motion accelerographs have been installed to continuously monitor the signals that satisfy event detection criteria. A trigger level of 0.02% of the full-scale (2 g) and a sampling of 200 samples per second are set for the data recording. The dynamic range of the systems is 108 dB at 200 samples/s with 18-bit resolution. The data for 80 local earthquakes (3 M_L 5.6) have been recorded during 1998–2003 shown in Figure 1 *a* with a N–S depth section on GIS platform in Figure 1 *b*. The depth section exhibits major clustering of events along Main Boundary Thrust (MBT) and in its proximity. The composite fault plane solution from the strong motion events along MBT suggests thrust faulting with strike slip component with a dip of 35°NNE striking at 310 (USGS convention) (Figure 1 *b*). Since the fault types are similar due to clustering along MBT, no fault term has been introduced in our attenuation models. In Figure 2 *a–c* the Butterworth band-pass filtered accelerograms at station Mangan are presented for the event 0010181422 (M_L = 4.9). The Fourier spectra of S-envelope (S) and the background/pre-event trace (B) windows are displayed in Figure 2 *d–f* in log–log scale in order to depict the quality of the data used in the analysis.

Following Andrews[12] the amplitude spectrum of the ith event recorded at the jth station for the kth frequency,

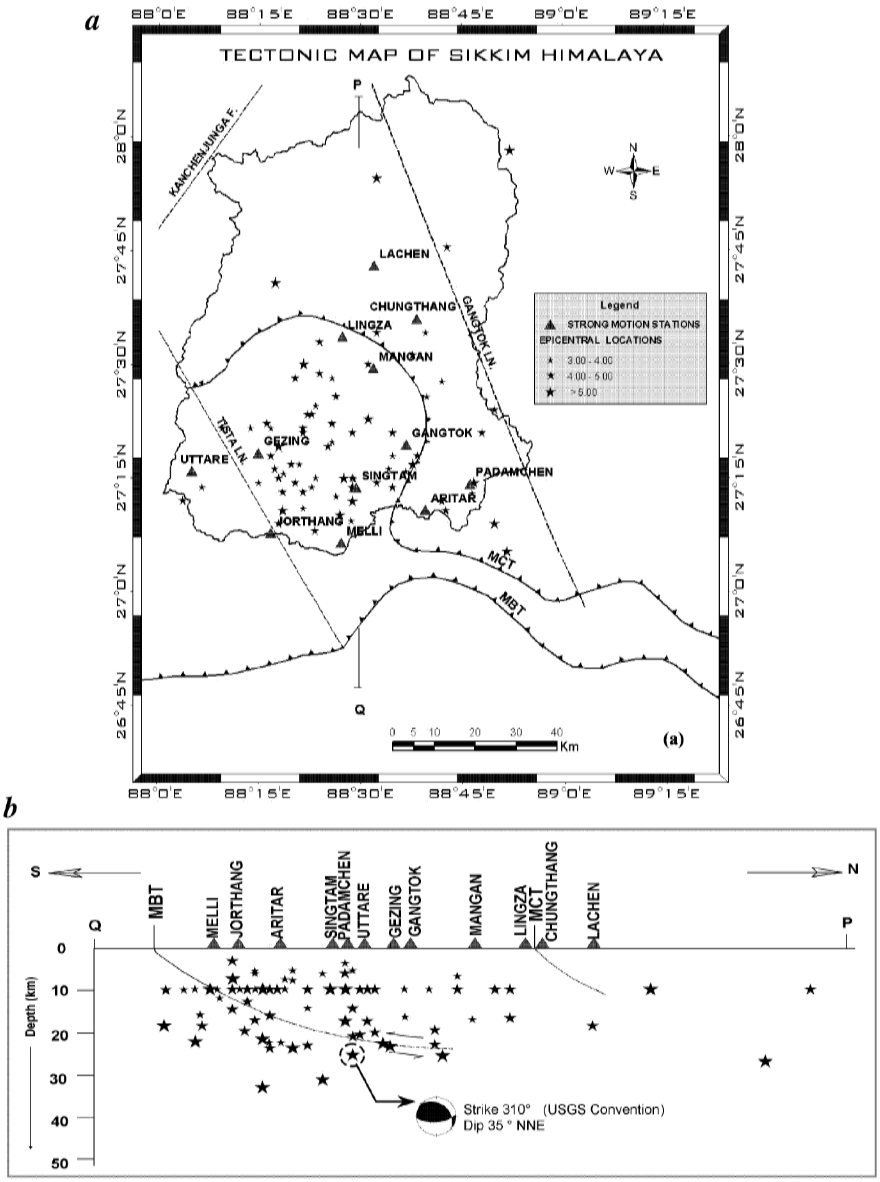

Figure 1. ***a***, Eighty earthquakes located in the Sikkim–Darjeeling area recorded by the Sikkim Strong Motion Array (SSMA) with $3.0 \leq M \leq 5.6$. ***b***, N–S depth-section on GIS platform showing the subsurface distribution of these earthquakes along with the composite fault plane solution that exhibits thrust faulting with strike-slip component.

$A(r_{ij}, f_k)$ can be written in the frequency domain as a product of a source spectral function $SO_i(f_k)$, a propagation path term $P(r_{ij}, f_k)$, and a site spectral function $SI_j(f_k)$ (refs 13–15),

$$A(r_{ij}, f_k) = SO_i(f_k).\, SI_j(f_k).\, P(r_{ij}, f_k). \tag{1}$$

The propagation path term can be expressed as,

$$P(r_{ij}, f_k) = G(r_{ij}) e^{\frac{-(\pi f_k r_{ij})}{Q_s(f_k)\beta}}, \tag{2}$$

where $G(r_{ij})$ accounts for geometrical spreading, $Q_s(f_k)$ and β are S-wave frequency-dependent quality factor of the medium in the study region and velocity, respectively. We assumed $\beta = 4.0$ km/s as an average shear-velocity on the basis of the velocity models for the Sikkim Himalaya and $\alpha/\beta = 1.73$, where α is the P-wave velocity[16]. We considered[17,18],

$$G(r_{ij}) = \frac{1}{r_{ij}} \quad \text{for } r < 100 \text{ km},$$

or,

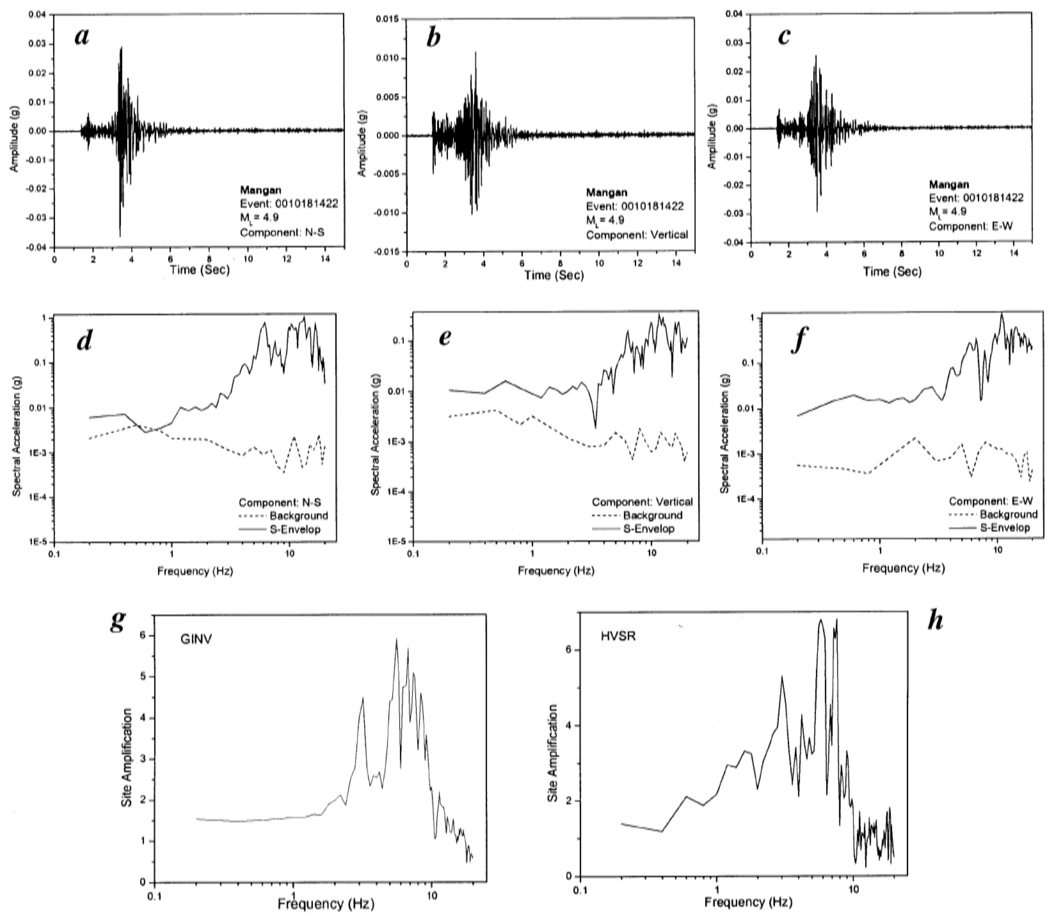

Figure 2. Butterworth band-pass filtered accelerograms of three components at Mangan station for the event 0010181422 ($M_L = 4.9$). ***a***, NS; ***b***, Vertical; and ***c***, EW. Fourier spectra of S-envelope (S) and Background (B) for ***d***, NS, ***e***, Vertical and ***f***, EW. Site response at Mangan computed through ***g***, HVSR and ***h***, GINV.

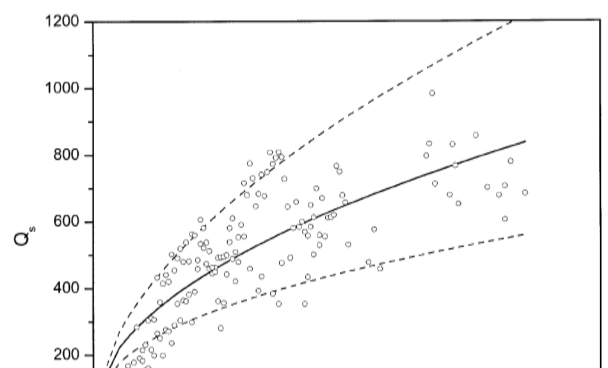

Figure 3. Plot of Q_S vs frequency. The dashed lines represent the zone of scatter of the data points with respect to the power law relation between Q_S and frequency with ± 1 standard deviation in the constant and the exponent.

$$G(r_{ij}) = (r_{ij} * 100)^{-0.5} \quad \text{for } r > 100 \text{ km}, \tag{3}$$

to take into account possible arrival of surface waves in the windowed data.

We have determined Q_s and its dependence on frequency in the form of a power law through regression analysis of the direct S-wave data recorded by SSMA as shown in Figure 3. The power law can be expressed as given below

$$Q_s = (167.69 \pm 28.25) f^{(0.47 \pm 0.06)}. \tag{4}$$

Site response has been estimated through Generalized Inversion (GINV) approach and HVSR technique[14,15,19,20], these techniques are considered apt in the absence of a reference site. The sample site response curves by HVSR and GINV at Mangan for the source azimuth of 197.13°N are presented in Figure 2 *g* and *h* respectively. In order to illustrate spatial distribution of site response in the Sikkim Himalaya, we subdivided HVSR values in three frequency bands, namely, low frequency band, LFB (≤5 Hz) with a geometric

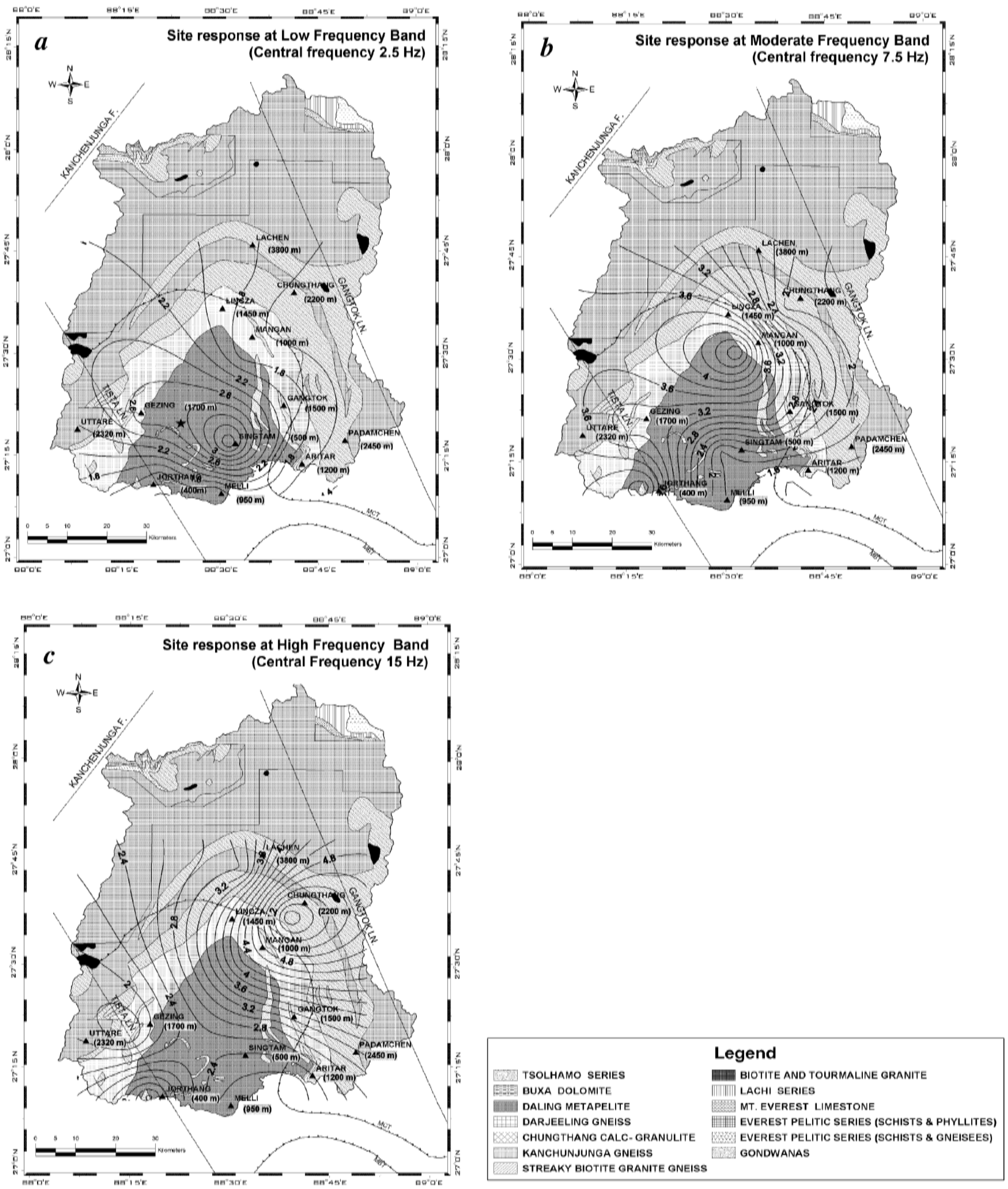

Figure 4. Spatial distribution of site response at the geometrical central frequencies. ***a***, 2.5 Hz for the Low frequency band, LFB ($f < 5$ Hz); ***b***, 7.5 Hz for the moderate frequency band, MFB ($5 \leq f < 10$ Hz); ***c***, 15 Hz for the High frequency band, HFB ($10 \leq f <$ 20 Hz). Background constitutes the geological map of the Sikkim Himalaya.

central frequency 2.5 Hz, moderate frequency band, MFB (5–10 Hz) with a geometric central frequency 7.5 Hz and high frequency band, HFB (10–20 Hz) with a geometric central frequency 15 Hz. The averaged site response values at these frequencies are plotted, contoured and presented in Figure 4 *a–c* respectively. It is observed that high site response contours at LFB are at the foothills of the Himalayas in the Siwalik soft rock terrain. Maximum site amplification to the tune of 3.4 is observed near Singtam that is at an elevation of 500 m above mean sea level. It is further evident from Figure 4 *a* that as the altitude increases towards the northern districts of Sikkim, namely, Mangan, Chungthang and Lachen with the elevations of 1000, 2200 and 3800 m respectively, the site response diminishes. For the MFB with the geometrical central frequency of 7.5 Hz we observe in Figure 4b a different scenario of spatial variation of site amplification in contrast to that at low frequency band. Here, the higher HVSR values peak near Mangan at an elevation of 1000 m. In this region the hill slope is much steeper, the maximum site amplification observed in this case is 4.6. In the HFB with geometric central frequency 15 Hz the spatial variation pattern of site amplification shifts further northeast towards Chungthang with an altitude of 2200 m, site response peaking to a value of 5.8 on the high hill scarp between Mangan and Chungthang. It is noted that the Gangtok lineament is striking very close to Chungthang and is seismogenic in the area. This variation in the SR contour pattern at three distinct frequency bands seem to follow the topography for the moderate to high frequency regime and is in consistence with the findings of Bouchon and Barker[21], when they simulated an experiment to observe ground motion amplification at or near top of the hill depending on the slope and the resonance frequency of the respective morphometric signature of the terrain. We simulated source spectra assuming Brune's source model[22,23] that is given as,

$$\overline{SO_i}(f_k) = \frac{[R_{\theta\phi} F(2\pi f_k)^2]}{\sqrt{2}(4\pi\rho\beta^3)} \dot{M}_{oi}(f_k), \quad (5)$$

where $R_{\theta\phi}$ (= 0.63) is the radiation pattern averaged over an appropriate range of azimuths and take-off angles, F (= 2.0) accounts for the amplification of the seismic wave at the free surface, ρ is the crustal density of the continental crust at the focal depth, β is the shear-wave velocity at the source region and $\dot{M}_{oi}(f_k)$ is the moment rate spectrum. The factor $\sqrt{2}$ accounts for the partition of S-wave energy into transverse components. We have assumed $\tilde{n}$ to be equal to 2.7 g/cc (crustal density) and β = 4.0 km/s[16]. The moment rate spectrum $\dot{M}_{oi}(f_k)$ can be expressed as,

$$\dot{M}_{oi}(f_k) = \frac{M_{oi}}{1+(f_k/f_{ci})^{\gamma_i}}, \quad (6)$$

where M_{oi}, f_{ci} and γ_i respectively are the scalar moment, corner frequency and the high frequency spectral fall-off associated with the ith earthquake. The value of corner frequency f_{ci} can be computed using the relation[23],

$$f_{ci} = 4.9*10000*\beta*\left(\frac{\Delta\sigma}{M_0}\right)^{1/3}. \quad (7)$$

Kanamori's relation[24] that is given below can be used to compute M_0 from M_L.

$$M_W = 2/3 \log(M_0) - 10.73, \ (M_0 \text{ in dyne-cm}). \quad (8)$$

To estimate the value of stress drop ($\Delta\sigma$) we used the relation[24],

$$\log(M_0) = 3/2 \log(S) + \log(16\Delta\sigma / 7\pi^{3/2}), \quad (9)$$

where S represents the surface area, that can further be calculated using the relation[25],

$$\log(S) = 1.21\, M_s - 5.05 \ (S \text{ in square km}). \quad (10)$$

Since we have recorded M_L, we convert it to surface wave magnitude (M_S) using the equation,

$$0.80\, M_L - 0.60\, M_S = 1.04. \quad (11)$$

We can, therefore, establish an empirical relation between f_{ci} and M_W (since below 5.5, M_W and M_L are almost equal)[4]. Frequencies thus estimated closely correspond to the frequencies obtained by inversion of the observed data, hence, considering it appropriate to obtain f_{ci} from above set of relations for the purpose of simulation. In the process of inversion we also obtained values of scalar moment M_0 that were related to moment magnitude M_W through the following empirical relationship.

$$\log(M_0) = 2/3\, M_W + (9.91 \pm 0.45) \ (M_0 \text{ in dyne-cm}). \quad (12)$$

Having determined all the terms on the right hand side of eq. (1) we used the convolution model to generate the acceleration spectra.

An evaluation of seismic hazard requires an estimate of expected ground motion at the site of interest. In its most fundamental form, an attenuation relation[4] can be described by its more common logarithmic form,

$$\ln(Y) = C_1 + C_2 M - C_3 \ln(r) - C_4 r + C_5 F + C_6 S + \varepsilon, \quad (13)$$

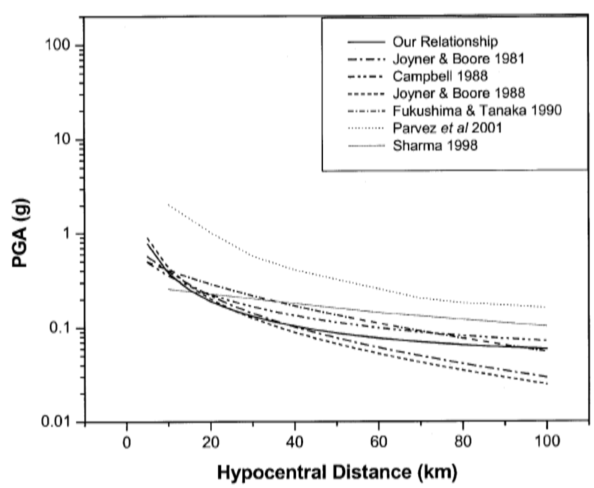

Figure 5. Comparison between different attenuation relationships for M_W = 7 and hypocentral distances varying up to 100 km.

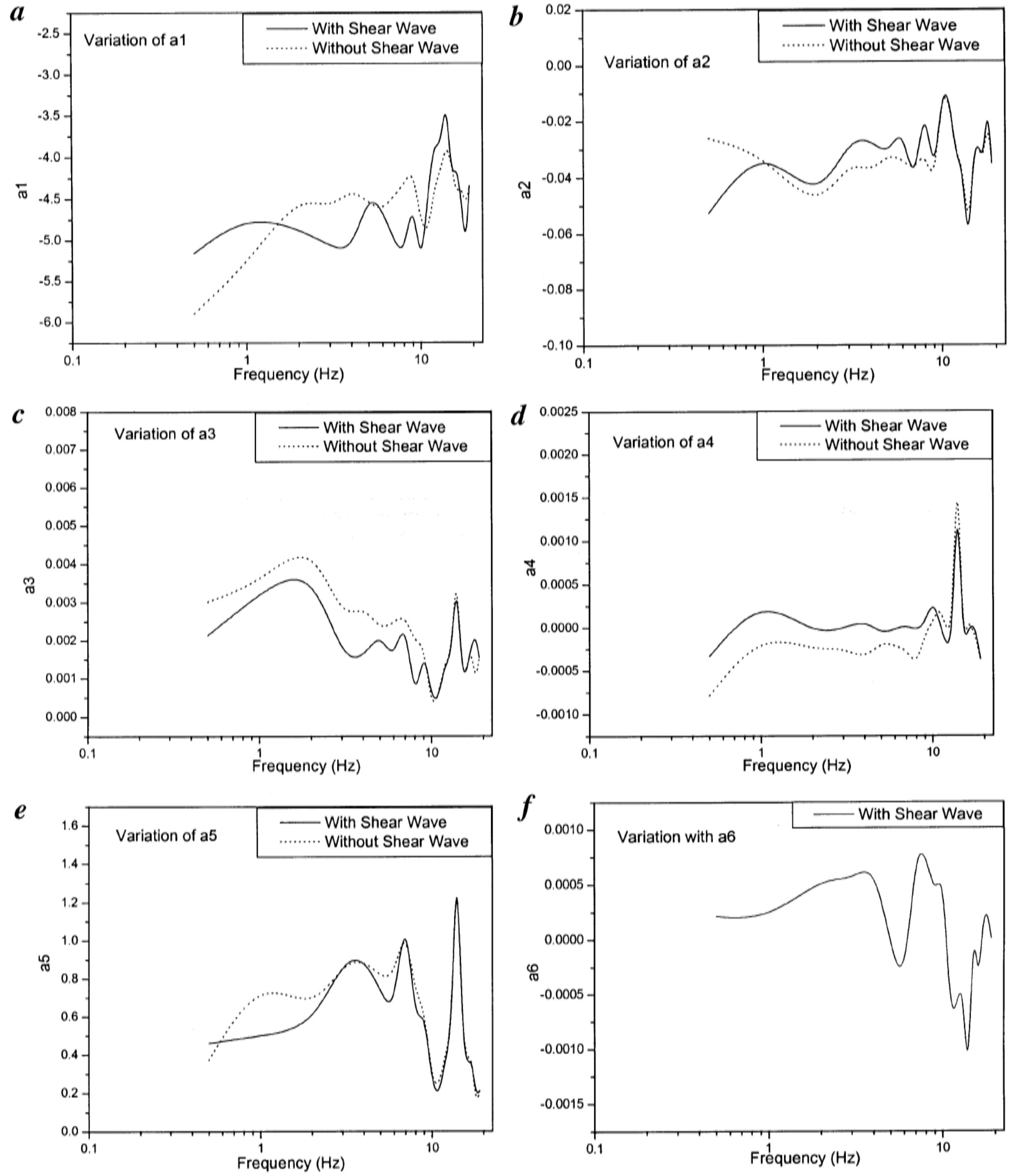

Figure 6. Spline smoothened variation of different coefficients in the spectral attenuation relations with frequency.

where Y is the strong motion parameter of interest (PGA in this case), M is the earthquake magnitude, r is a measure of source-to-site distance, F a parameter characterizing type of faulting, S the parameter characterizing local site condition, and ε is the random error term. Ignoring the site and fault parameter, the generalized attenuation law takes the form,

$$\ln(Y) = C_1 + C_2 M - C_3 \ln(r) - C_4 r. \quad (14)$$

We have used a semi-empirical approach by selecting to minimize the difference between observed and predicted values of ground motion, starting with eq. (14). Thus the first order attenuation relation takes the form:

$$\ln(Y) = -3.6 + 0.72M - 1.08\ln r + 0.007r. \quad (15)$$

This is a mean attenuation relationship without considering local site conditions and for hypocentral distances less than 100 km. A comparative plot between our 1st order relationship, Joyner–Boore relationship[5,6], Campbell's relation[26], Fukushima–Tanaka relationship[8], relationship given by Sharma[1] and Parvez *et al.*[2] for $M_W = 7$ and varying hypocentral distances from 0 to 100 km is shown in Figure 5. Our

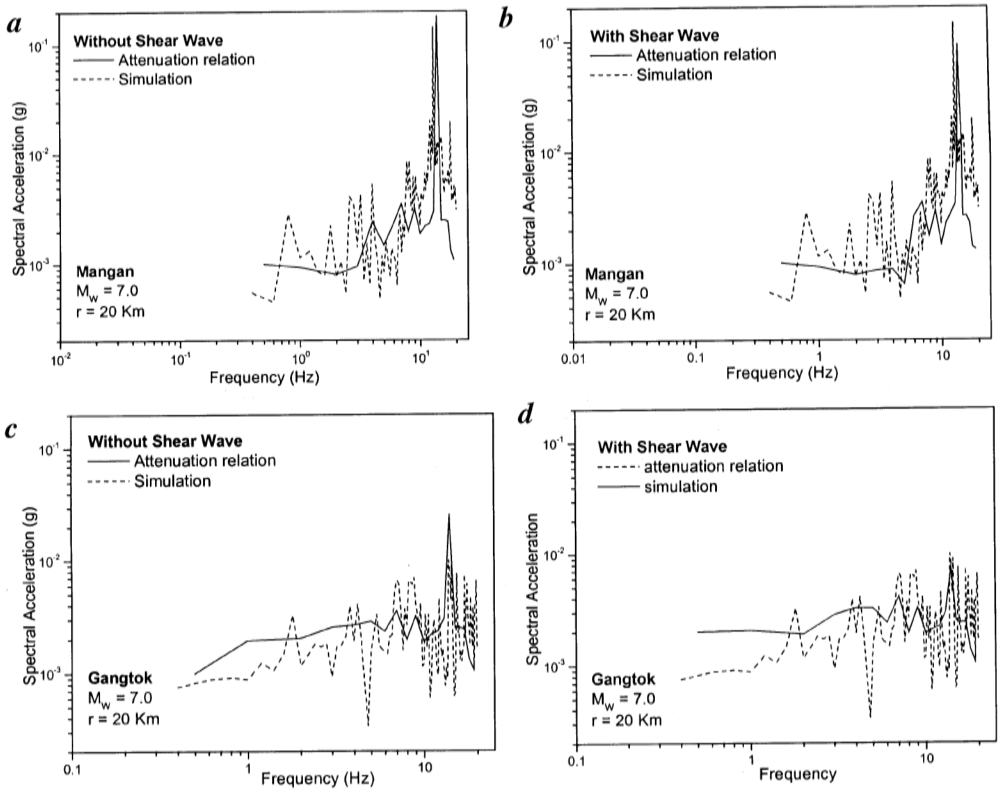

Figure 7. Comparative plots of simulated spectral acceleration using the Brune's source model and by the spectral attenuation relations within the frequency band 0.5–19 Hz at Mangan. ***a***, without shear wave velocity; ***b***, with shear wave velocity and at Gangtok; ***c***, without shear wave velocity and ***d***, with shear wave velocity.

1st order relation fits well into this set of attenuation laws. Since we have already observed in our previous analysis that the spectral acceleration depends on site amplification, topography, the source azimuth and the local site conditions, it became necessary for us to work out a local attenuation relation starting with the general form of equation given by Campbell's Attenuation law[7] for spectral acceleration,

$$\begin{aligned}\ln(SA_{\mathrm{H}}) = \ln(A_{\mathrm{H}}) + c_1 + c_2 \tanh[c_3(M-4.7)] \\ +(c_4 + c_5 M)r + .5c_6 S_{\mathrm{SR}} + c_7 \tanh(c_8 D) \\ (1-S_{\mathrm{HR}}) + f_{\mathrm{SA}}(D) + \varepsilon,\end{aligned} \tag{16}$$

where SA_{H} is the horizontal spectral acceleration, A is the PGA, S_{SR} and S_{HR} are variables representing local site conditions for soft rock and hard rock respectively, D is the depth to the basement rock and f_{SA} is a function of D.

Since in our study region, the sediment cover is very thin, we neglected the terms corresponding to hard rock and soft rock, instead we introduced a term of site amplification to take into account local site conditions. Moreover, being situated in a hilly terrain dependence on topography is expected, and to account for this we have introduced a term for station elevation. Our established second order attenuation relation, therefore, takes the following shape,

$$\begin{aligned}\ln(\mathrm{PGA}) = \ln(\mathrm{SA}) - a1 - (a2 + a3M_{\mathrm{W}})r \\ - a4h - a5 \ln(SR),\end{aligned} \tag{17}$$

where h is the site elevation, SR the RMS site response and SA is the spectral acceleration at respective frequencies for which the relation holds well. A set of spectral attenuation relations for frequencies between 0.5 and 19 Hz has been determined at different source azimuths. It is to be noted that due to the paucity of data within the magnitude range 5.6 to 8.3 (MCE)[3] we simulated the spectral acceleration at these magnitudes and clubbed with the recorded event spectra. As expected, the site amplification and spectral acceleration are balancing the azimuthal changes in the attenuation relations thereby stabilizing the coefficients to a large extent. We could further modify the relationship achieved in eq. (17) by appending a term S_{V} for the shear wave velocity in spite of a thin soil cover. The equation thereupon took the following shape,

$$\begin{aligned}\ln(\mathrm{PGA}) = \ln(SA) - a1 - (a2 + a3M_{\mathrm{W}})r \\ - a4h - a5 \ln(SR) - a6S_{\mathrm{V}}.\end{aligned} \tag{18}$$

Figure 6 shows the spline smoothened variation of different coefficients as a function of frequency. On comparison, the coefficients of the attenuation relationship (17) show minor variation with respect to the ones of eq. (18) as are evident from Figure 6.

In order to judge the authenticity of these attenuation relations we attempted to simulate spectral acceleration using the Brune's source model[23] and also by using both the attenuation relations (17) and (18) within the frequency band 0.5–19 Hz at all the nine sites, the results at Mangan and Gangtok being presented in Figure 7. It is to be noted that the spectral simulation considered around 100 frequency samples while the attenuation relation considered 20 discrete samples within the same frequency band. As a result, the spectral acceleration computed through attenuation relations mimics the mean trend of that simulated by Brune's source model as depicted in Figure 7, with and without shear wave velocity term in the spectral attenuation models. No major change is observed in the computed spectral acceleration curves with or without shear wave velocity term in the relationships.

It is, therefore, evident that the recommended spectral attenuation relations developed here are the characteristic spectral attenuation models in the Sikkim Himalaya for predicting free-field amplitudes of horizontal component of Peak Ground Acceleration for moderate to large earthquakes with a hypocentral distance less than 100 km.

1. Sharma, M. L., Attenuation relationship for estimation of peak ground horizontal acceleration using data from strong motion arrays in India. *Bull. Seismol. Soc. Am.*, 1998, **88**, 1063–1069.
2. Parvez, I. A., Gusev, A. A., Panza, G. F. and Petukhin, A. G., Preliminary determination of interdependence among strong motion amplitude, magnitude and distance for the Himalayan region, *Geophys. J. Int.*, 2001, **144**, 577–596.
3. Vyas, M., Nath, S. K., Pal, I., Sengupta, P. and Mohanty, W. K., GSHAP revisited for the prediction of maximum credible earthquake in the Sikkim region., *Acta Geophys. Polonica*, 2005, **53**, (in press).
4. Chen, W. F. and Scawthorn, C., *Earthquake Engineering Handbook*, CRC Press, 2003.
5. Joyner, W. B. and Boore, D. M., Peak horizontal acceleration and velocity from strong motion records including records from the 1979 Imperial Valley, California, earthquake. *Bull. Seismol. Soc. Am.*, 1981, **71**, 2011–2038.
6. Joyner, W. B. and Boore, D. M., Measurement, characterization, and prediction of strong motion. Earthquake Engineering and Soil Dynamics: 2. Recent Advances in Ground Motion Evaluation, ASCE NY, 1988, pp. 43–102.
7. Campbell, K. W., Empirical near-source attenuation relationships for horizontal and vertical components of peak ground acceleration, peak ground velocity, and pseudo-absolute acceleration response spectra. *Seismol. Res. Lett.*, 1997, **68**, 154–177.
8. Fukushima, Y. and Tanaka, T., A new attenuation relation for peak horizontal ground acceleration of strong ground motion in Japan. *Bull. Seismol. Soc. Am.*, 1990, **80**, 757–783.
9. Bolt, B. A., *Earthquake and Geological Discovery*, Scientific American Library, New York, 1993.
10. Nath, S. K., Chatterjee, D., Biswas, N. N., Dravinski, M., Cole, D. A., Papageorgiou, A., Rodriguez, J. A. and Poran, C. J., Correlation study of shear wave velocity in near surface geologic formations in Anchorage, Alaska. *Earthq. Spectra*, 1997, **13**, 55–75.
11. National Bureau of Soil Survey, Master plan for irrigation development, Sikkim, Govt. of Sikkim, Report, Agricultural Finance Corporation Ltd., 1994, pp. 35–47.
12. Andrews, D. J., Objective determination of source parameters and similarity of earthquakes of different size. *Earthquake Source Mechanics*, American Geophysical Union, Washington DC, 1986, pp. 259–268.
13. Lermo, J. F., Francisco, S. and Chavez-Garcia, J., Site effect evaluation using spectral ratios with only one station. *Bull. Seismol. Soc. Am.*, 1993, **83**, 1574–1594.
14. Nath, S. K., Biswas, N. N., Dravinski, M. and Papageorgiou, A., Determination of S-wave site response in Anchorage, Alaska in the 1–9 Hz frequency band. *Pure Appl. Geophys.*, 2002, **159**, 2673–2698.
15. Nath, S. K., Sengupta, P. and Kayal, J. R., Determination of site response at Garhwal Himalaya from the aftershock sequence of 1999 Chamoli Earthquake. *Bull. Seismol. Soc. Am.*, 2002, **92**, 1071–1081.
16. De, R., A microearthquake survey in the Himalayan foredeep region, Sikkim Himalaya. *J. Geophys.*, 2000, **XXI**, 1–8.
17. Ordaz, M. and Singh, S. K., Source spectra attenuation of seismic waves from Mexican earthquakes and evidence of amplification in the hill zone of Mexico City. *Bull. Seismol. Soc. Am.*, 1992, **82**, 24–43.
18. Castro, R. R., Pacor, F., Sala, A. and Petrungaro, C., S-wave attenuation and site effects in the region of Friuli, Italy. *J. Geophys. Res.*, 1996, **101**, 22355–22369.
19. Nath, S. K., Sengupta, P., Sengupta, S. and Chakarabarti, A., Site response estimation using strong motion network: A step towards microzonation of Sikkim Himalayas. *Curr. Sci.*, 2000, **79**, 1316–1326.
20. Nath, S. K., Sengupta, P., Srivastav, S. K., Bhattachayra, S. N., Dattatrayam, R. S., Prakash, R. and Gupta, H. V., Estimation of S-wave site response in and around Delhi region from weak motion data. *Proc. Indian Acad. Sci.* (*Earth Planet. Sci.*), 2003, **112**, 441–462.
21. Bouchon, M. and Barker, J. S., Seismic response of a hill: The example of Tarzana, California. *Bull. Seismol. Soc. Am.*, 1996, **86**, 66–72.
22. Dutta, U., Biswas, N., Martirosyan, A., Papageorgiou, A. and Kinoshita, S., Estimation of earthquake source parameters and site response in Anchorage, Alaska from strong-motion network data using generalized inversion method. *Phys. Earth Planet. Int.*, 2003, **137**, 13–29.
23. Hwang, H. H. M. and Huo, J. R., Attenuation relations of ground motion for rock and soil sites in Eastern United States. *Soil Dynam. Earthquake Eng.*, 1997, **16**, 363–372.
24. Kanamori, H. and Anderson, D. L., Theoretical basis of some empirical relations in seismology. *Bull. Seismol. Soc. Am.*, 1975, **65**, 1073–1095.
25. Bath, M. and Duda, S. J., Earthquake volume, fault plane area, seismic energy, strain, deformation and related quantities. *Ann. Geofis.* (*Rome*), 1964, **17**, 353–368.
26. Campbell, K. W., Predicting strong ground motion in Utah. In *Evaluation of Regional and Urban Earthquake Hazard Risks in Utah* (eds Hays, W. W. and Gori, P. L.), USGS Professional Paper, 1988, pp. L1–L31.

ACKNOWLEDGEMENTS. This work is a part of an ongoing project 'Microzonation of Sikkim Region' that has been funded by Seismology Division of the Department of Science and Technology, Government of India since 1998. We thank both the reviewers for their critical review of the manuscript and valuable suggestions.

Received 28 July 2004; revised accepted 1 December 2004